Article

Phenol-Furfural Resin/Graphite/Ag Based Electrically Conductive Adhesive Composites from Waste Bagasse with Enhanced Thermo-Electric Properties

Syeda Mahnoor Zehra [1], Maryam Bibi [1], Azhar Mahmood [1,*], Abraiz Khattak [2], Muhammad Zeeshan Asad [3] and Syeda Hijab Zehra [4]

[1] School of Natural Sciences, National University of Sciences and Technology, H-12, Islamabad 44000, Pakistan; syedamahnoor1111@gmail.com
[2] US Pakistan Center for Advanced Studies in Energy, National University of Sciences and Technology, H-12, Islamabad 44000, Pakistan
[3] Loughborough University, Loughborough LE11 3TU, United Kingdom
[4] Department of Earth and Environmental Science, Bahira University Islamabad Campus H-11, Islamabad 44000, Pakistan
* Correspondence: dr.azhar@sns.nust.edu.pk; Tel.: +92-51-9085-5574

Abstract: This study endeavors the preparation and evaluation of Phenol Furfural Resin (PFR) from bagasse and its nanocomposites for Electrically Conductive Adhesives (ECAs) application. PFR was prepared with the furfural extracted from bagasse using modified acid digestion method. Three different formulations of PFR nanocomposites with conductive nanoparticles i.e., PFR-silver, PFR-graphite, and PFR-silver + graphite were prepared using 20-60 w/w% of fillers via impregnation method. Resultant products were characterized by FT-IR, SEM, EDS and XRD spectroscopy. Electrical conductivity was measured using four probe technique while band gap was calculated via Tauc plot. Virgin PFR has shown poor conductivity up to 2.6×10^{-4} Scm^{-1} while the highest conductivity achieved was 8.2×10^{-1} Scm^{-1} for nanocomposite constituted silver, graphite, and PFR with 40:30:20 ratios respectively. This synergism was exhibited because graphite and Ag NPs supply excellent junctions for building networks. Both tend to coalesce due to van der Waals forces and high surface energies, therefore conductive pathways numbers can be increased, and contact area can be effectively enlarged. This ternary composite has exhibited the lowest bandgap energy value i.e., 3.1 eV. Thermogravimetric temperatures T_0 and T_{deg} values were increased up to 120 °C and 484 °C respectively, showing significant increase in thermal stability. Therefore, the resultant nanocomposite material has good potential to be employed as ECAs in electronic industry.

Keywords: silver; green material; biomass; furfural; PFR; conductivity

1. Introduction

The current world economy is affected by scarcity of basic human necessities like clothing, shelter, domestic fuel, and food due to feedstock reserves depletion. Experts have been operational on different choices for exploring alternate ways for achieving better key solutions for such basic needs. In order to reduce the world's dependency on fossil fuel, the implementation of subsequent ways such as fuels from renewable resources, production of green materials and chemicals is now gaining strength [1–4].

With the advancement of science and technology, there is need for development of such electronic units which have portability, miniature size as well as have highly integrated functions [5]. Consequently, the electronic industry demands new interconnect bonding materials which have the ability to offer good electrical conductivity, satisfied thermal stability, flexibility along with low cost and environment friendliness. Polymers produced from renewable resources are also of great interest due to their lower cost and high abundance [6–8]. Electrically conductive adhesives (ECAs) are the

 doi:10.20944/preprints202306.0372.v1

excellent options for electronic industry to be used as an interconnection material since it offers improved electrical performance, fine pitch interconnect, environmental friendliness, and low processing temperatures [9]. Mainly the composition of ECAs is of two part one is polymeric and other is filler. Polymeric part may consist of polymeric resins such as polyurethane, polyimide, silicones, acrylates, epoxy, or phenolic resins etc. [10]. While the conductivity will be provided using conductive fillers such as Ag, Ni, graphite, graphene, CNTs etc. [11–13]. Various conductive fillers have been studied including zinc complexes [14,15], metal oxide [16] cadmium [17], cobalt nanoparticles [18], and so on. However, some issues like poor interconnection between polymer resin and conductive fillers and aggregation are to be addressed. Suherman et al., has reported 28 Scm^{-1} Suherman based upon 80% graphite with epoxy [19]. The research group of Duarte and Paulo [12] have studied epoxy resin composites consist of single & multiwalled carbon nanotubes (SWCNT & MWCNT) calculated volume resistivity of about 1×10^{1} and 1×10^{6} Ω.cm for SWCNT & MWCNT. In another work Dhakate *et al*. [20] have deliberated graphite (natural and synthetic) as the conductive material with epoxy resin for bipolar plates with the highest conductivity of about 150 Scm^{-1}. Nayak along with co-mates [21] have extensively reviewed adhesives resins with various conductive fillers and reported thermal conductivity of 0.45 W/m.K. and 10^{1} Scm^{-1} as electrical conductivity for epoxy/single wall nanotubes of carbon based ECAs. Tang et al. [22] designed and synthesized Silicone resin with functional silane and applied this as silver conducting inks, where Ag-silicone resin with 53.93 wt.% Ag shows the lowest resistivity of 1.43×10^{-6} Ωm which was then applied as the conductive silver ink.

In the present work, ECAs were prepared by incorporation of graphite and Ag nanoparticles into matrix of PFR. Graphite nanoparticles can fill the gap between the unattached Ag NPs, and new conductive paths are well formed by linking the gap between Ag NPs. Graphite and Ag NPs supply excellent junctions for building networks, both of these tend to coalesce during various applications due to van der Waals forces and high surface energies, therefore conductive pathways numbers can be increased and contact area can be effectively enlarged [23].

2. Materials and Methods

2.1. Materials

Sugarcane plant was purchased from local market of city Wah Cantt, Pakistan. It was first washed then allowed to pass through the sugarcane presser to obtain bagasse. Subsequently, this bagasse was shade dried for about 14 days followed by grinding and drying in oven at about 50 ^{o}C for half an hour to ensure its moisture free. Chloroform (99%), $AlCl_3{\cdot}6H_2O$ (99%), HCl (37%), NaCl (99%), KOH (99%), Phenol (99%), Urea (99%), Hydrazinium chloride (99%), Silver Nitrate (99%), Graphite (dry battery cells) were used. All the chemicals were procured from Daejung, Korea while deionized water was used for all the solution preparations.

 doi:10.20944/preprints202306.0372.v1

2.2. Furfural extraction from bagasse

A mixture of catalysts comprising of equal quantity of NaCl and $AlCl_3.6H_2O$ was prepared. 12% HCl solution along with 2 w/v% of the catalyst material was used as an extraction medium. Bagasse was charged in 1:10 proportion of extraction medium, it was then mixed and agitated to make sure proper mixing of solution and powder. Subsequently the prepared material was poured into a 1000 mL round bottom flask attached with condenser and heated at 100°C for 2.5 hours with magnetic stirring in electrothermal heating mantle. After the bagasse digestion, distillate was transferred into a separating flask. Chloroform was added into distillate and shaken well to extract furfural into chloroform phase. Evaporation of chloroform by rotary evaporator yielded 53% furfural.

2.3. Synthesis of Phenol-Furfural Resin

Phenol furfural resin was prepared according to the method reported by Zeeshan *et al*. [24]. Furfural and Phenol were reacted in molar ratio of 0.9:1. About 12.5 g of phenol and 0.25 g of KOH as catalyst was taken into 100 mL three necked round bottom flask and both were melted at 45 °C until KOH was dissolved. Subsequently, furfural (11.5 g) was dropwise added in about 30 minutes into flask with constant stirring. The temperature of the system was raised up to 135 °C for about 2 hours and solid product having dark colour was obtained. To cease the polymerization and to remove unreacted phenol, the product was placed in oven for 24 hours.

2.4. Graphite Powder

The graphite rod of 3A battery cell was dismantled, and grinded followed by sieving using nanometer pour sized sieve. This fine powder was used for the conductive nanocomposite synthesis.

2.5. Synthesis of Silver Nanoparticles

A simple approach of chemical reduction method [25] was used for the Ag NPs synthesis. Sodium hydroxide was used as an accelerator while hydrazinium chloride was used as the reducing agent. In the first step, 0.68 g of $AgNO_3$ was dissolved in 40 mL of DI water and kept at 90 °C for 5 minutes with vigorous stirring. Aqueous solutions of sodium hydroxide (0.64 g/10ml DI water) and hydrazinium chloride (0.45 g /10 ml DI water) were prepared and simultaneously added into silver nitrate solution where strong effervescence was noticed. This reaction was allowed to continue for about 1 hour until the fizziness disappeared. The obtained precipitates were washed with DI water for 5 times at speed of 5000 rpm to remove any kind of unreacted material and were dried in vacuum oven at 60 °C for 24 hours to obtained greyish silver nanoparticles.

The graphite rod of 3A battery cell was dismantled, and grinded followed by sieving using nanometer pour sized sieve. This fine powder was used for the conductive nanocomposite synthesis.

2.6. Preperation of Nanocomposite

2.6.1. Preparation of Graphite-Resin Nanocomposites

Graphite-resin nanocomposites were prepared in 20:60, 40:40, and 60:20 w/w ratios of graphite and PFR resin with the sample codes G-20, G-40, and G-60 respectively. For the impregnation of nanoparticles, mechanical stirring process was performed at 25 °C for 25 minutes. Afterward samples were placed in vacuum oven at 90 °C for 24 hours for the curing of resin. When the concentration of graphite powder was increased above 60 w/w ratio, saturation of particles was observed, and mechanical stirring became difficult. This results in nonhomogeneous composite formation along with weak interaction between nanoparticles and polymers.

 doi:10.20944/preprints202306.0372.v1

2.6.2. Preparation of Ag-Resin Nanocomposite

The silver and resin nanocomposite were prepared with the same procedure used for the graphite resin composite preparation. Samples were labeled as S-20, S-40, and S-60 for the compositions as 20:60, 40:40, and 60:20 w/w ratios of Ag and PFR resin.

2.6.3. Preparation of Graphite-Ag-Resin nanocomposite

For ternary composite preparation, both graphite and Ag nanoparticles were used as per aforementioned method. These are coded as SG-20, SG-30, and SG-40 for 20:40:40, 30:30:40, and 40:30:40 w/w ratios of silver, graphite, and PFR resin respectively.

3. Analysis Techniques

Perkin Elmer Spectrum 100 FT-IR Spectrometer (USA) was used in frequency range of 350-4000 cm^{-1} to study the characteristics peaks of resin and nanocomposites. KBr disc was used as sample holder material. BRUKER D8 advanced X-ray diffractometer (Russia) equipped with Cu K alpha 0.154 nm wavelength radiation sources was employed in theta range of 10 to 80° to examine the crystallinity of the filler materials. The surface topography of the nanocomposites was examined by JSM-6490A, JEOL (Japan) SEM instrument while images were captured at resolution scale of 10 μm and 1 μm. Thermogravimetric Analysis (TGA) was conducted via SDT 650 TA instrument (USA) under inert conditions. Initial temperature was 26°C and it brings up to 900°C with 10 °C/min ramp rate in inert nitrogen atmosphere. Jasco V-770 via UV-Visible Spectrophotometer (Japan) was used for the bandgap measurements via Diffuse Reflectance Spectroscopic Technique (DRS). Conductivity of the samples was measured by a four-point probe method via JANDEL RM3000 (United Kingdom) test unit. The technique was used to measure the resistivity of the samples from which the conductivity was calculated by taking the reciprocal of resistivity. A DC supply with constant current was used for all the measurements.

4. Results and Discussion

4.1. Fourier Transform Infrared (FTIR) Spectroscopy

The structure of furfural was confirmed by the band at 3026 cm^{-1} in the FTIR spectrum which is due to the Ar-H stretch as shown in Figure 1. The aldehyde group was confirmed by the presences of two symmetric and asymmetric (H-C=O) bond stretch at 2846 cm^{-1} and 2807 cm^{-1} [24]. Intense band at 1664 cm^{-1} is due to C=O stretch. Moreover, the two bands at 1566 cm^{-1} and 1462 cm^{-1} are corroborated by presence of aromatic ring C=C bond. Furan ring presence was assured by 1215 cm^{-1} bond stretch. While 1014 cm^{-1} band stretch reflects presence of C-H plane. =C-H out of plane bending vibration and C-H out of plane (monosubstituted) have exhibited stretching vibration at 929 cm^{-1} and 740 cm^{-1} respectively [24]. The resin was corroborated by absorption band at 3315 cm^{-1} due to -OH (Figure 2). The polymer containing furfural and phenol monomers exhibits aromaticity due to which stretching bands of Ar C-C, Ar-OH and Ar-H appeared at 1598 cm^{-1}, 3315 cm^{-1}, and 3041 cm^{-1} respectively. Bands at 741 cm^{-1} and 1472 cm^{-1} were of monosubstituted C-H out of plane and C=C present in the furan ring. The band appeared at 1214 cm^{-1} due to C-O moiety. The C-O-C asymmetrical stretching vibrations resulted in the 1169 cm^{-1} and 1066 cm^{-1} bands. All these bands have confirmed the successful synthesis of phenol furfural resin.

Preprints (www.preprints.org) | NOT PEER-REVIEWED | Posted: 6 June 2023 doi:10.20944/preprints202306.0372.v1

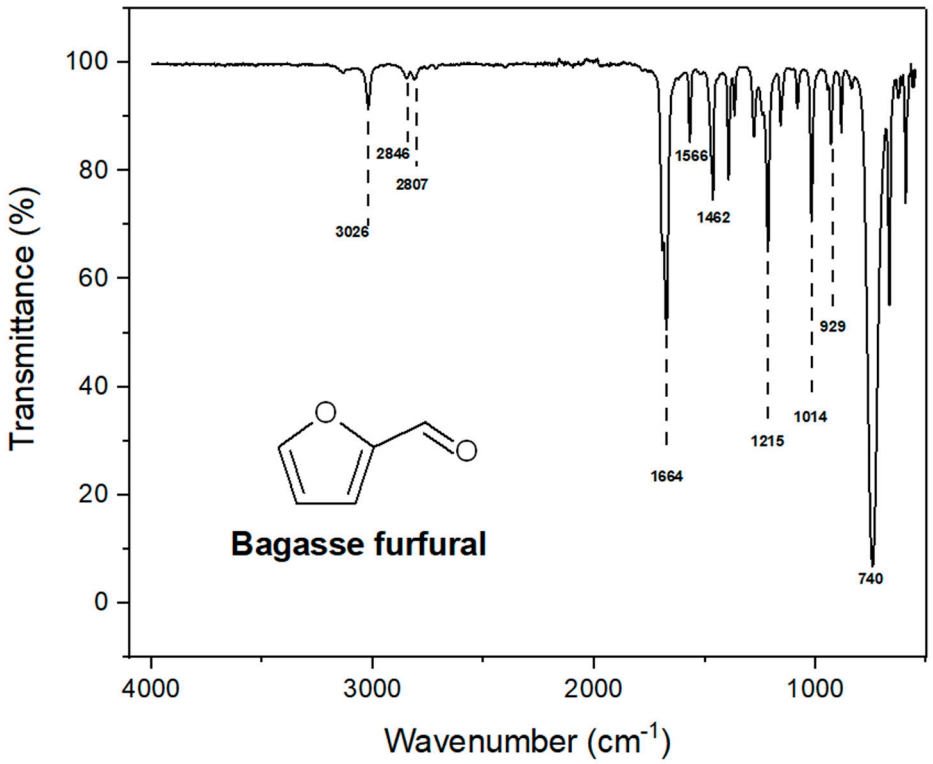

Figure 1. FT-IR spectrum of Furfural.

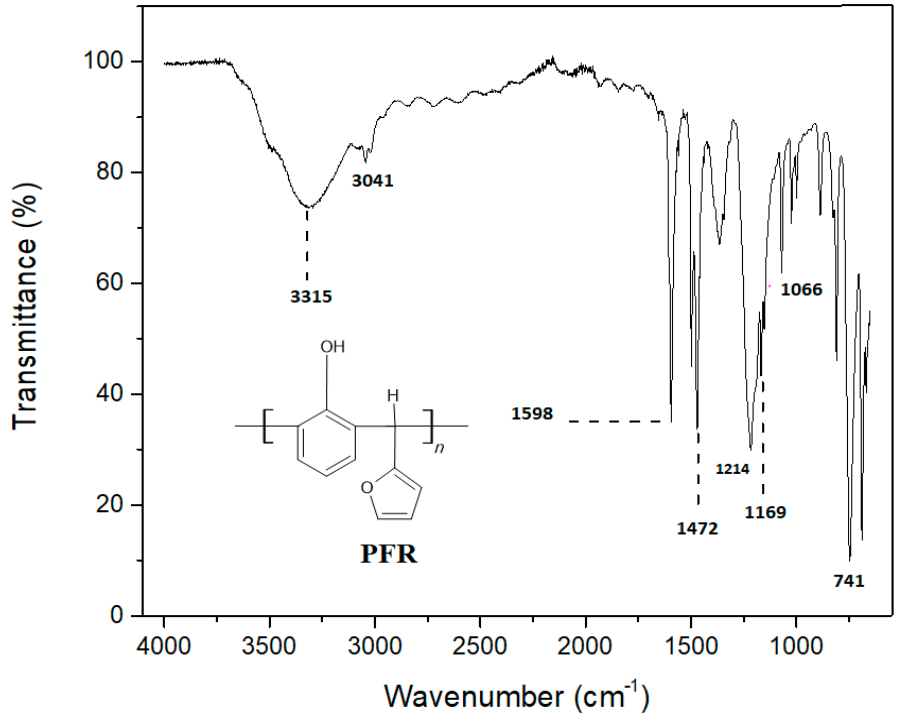

Figure 2. FT-IR spectrum of PFR.

4.2. X-Ray Diffractometry (XRD)

XRD results of PFR resin, graphite powder, and their composites were shown in Figure 3. The phenol furfural resin has depicted no sharp peak which has confirmed its amorphous nature. Similar result was reported by L Guo *et al*. [26]. On the other hand, sharp and intense peaks were shown by graphite and all of its composites. These peaks perfectly match JCPDS card no. 00-012-0212. The

Preprints (www.preprints.org) | NOT PEER-REVIEWED | Posted: 6 June 2023 doi:10.20944/preprints202306.0372.v1

intense characteristic diffraction pattern of pure graphite has exhibited two diffraction peaks one at 2θ value of 26.7° with interlaying spacing of 3.3Å and (002) plane while other at 2θ value of 54.5° having d-spacing 1.7 Å and (004) diffraction plane. The XRD results in Figure 3 depicted a detailed description of interlayer spacing and diffraction plane of graphite nanocomposites. The interlayer spacing of composites remained the same i.e., 3.3 Å, 1.7 Å for the two peaks respectively. This has confirmed that graphite particles remain unchanged even with mixing in phenolic resin and there is no reaction occurred in between the layers.

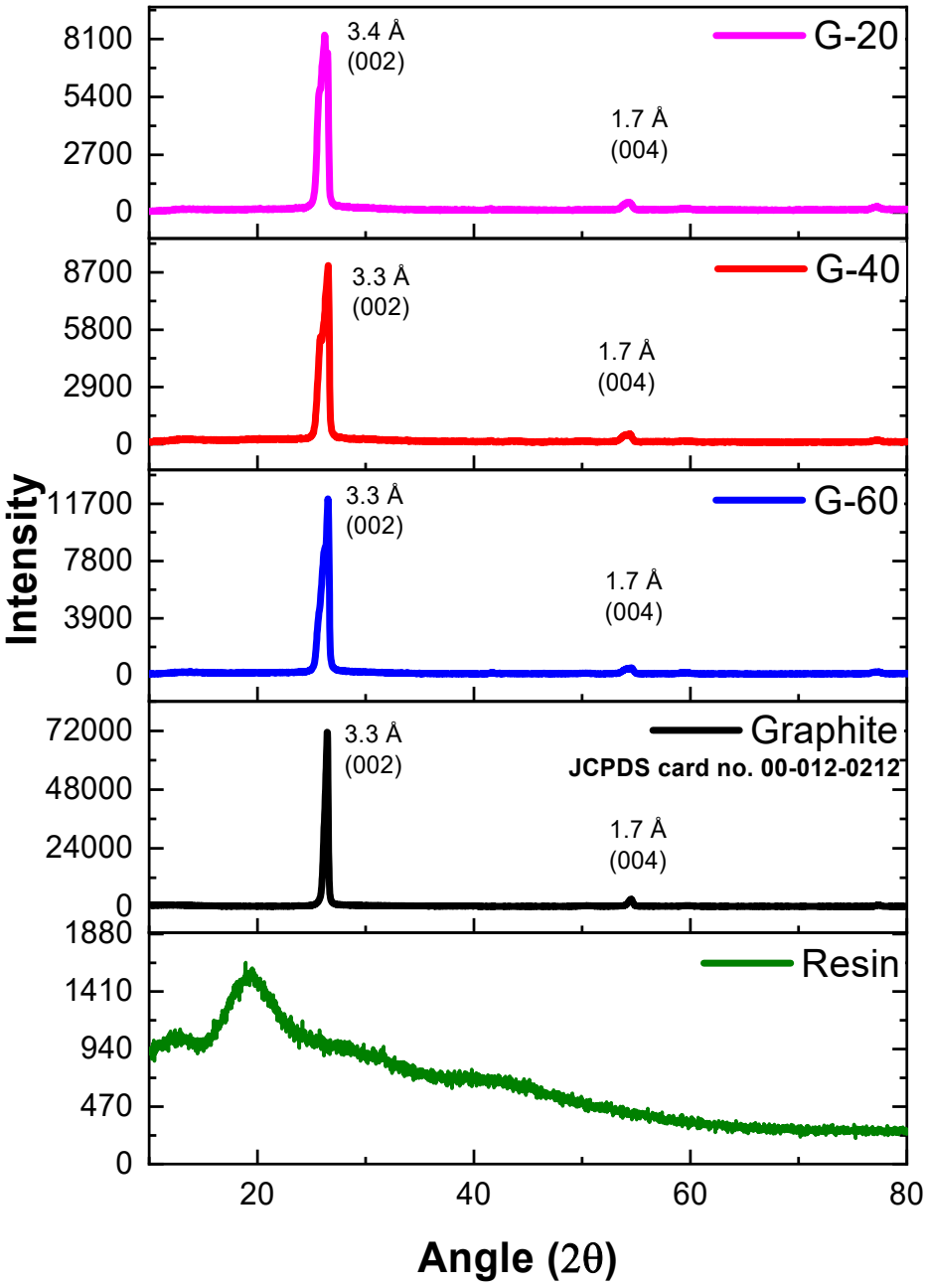

Figure 3. XRD pattern of resin and graphite composites.

Oxide free silver nanoparticles were characterized by XRD techniques (Figure 4). Ag nanoparticles have shown four intense and sharp diffraction peaks at 38.1°, 44.4°, 64.4°, and 77.4° reflecting 2.4 Å(111), 2.0 Å(200), 1.4 Å(220), and 1.2 Å(311) d-spacing (planes) respectively, are in agreement with that reported by Agasti [27] as well as perfectly matched with the literature JCPDS card no. 03–0931. While nanocomposites of Ag-resin have exhibited the same diffraction pattern with similar d-spacing values and diffraction planes. Figure 4 has exhibited 2θ and d-spacings values of

Preprints (www.preprints.org) | NOT PEER-REVIEWED | Posted: 6 June 2023 doi:10.20944/preprints202306.0372.v1

S-20 nanocomposite at 37.7° $d_{(111)}$ = 2.4 Å, 44.0° $d_{(200)}$ = 2.1 Å, 64.0° $d_{(220)}$ = 1.5 Å, 77.1° $d_{(311)}$ = 1.2 Å. While 2θ values were found at 38.1°, 44.0°, 65.1°, 77.1° and 38.1°, 44.1°, 64.2°, 77.1° for S-40 and S-60 respectively, having the similar diffraction planes and d-spacing values as of pure Ag nanoparticles.

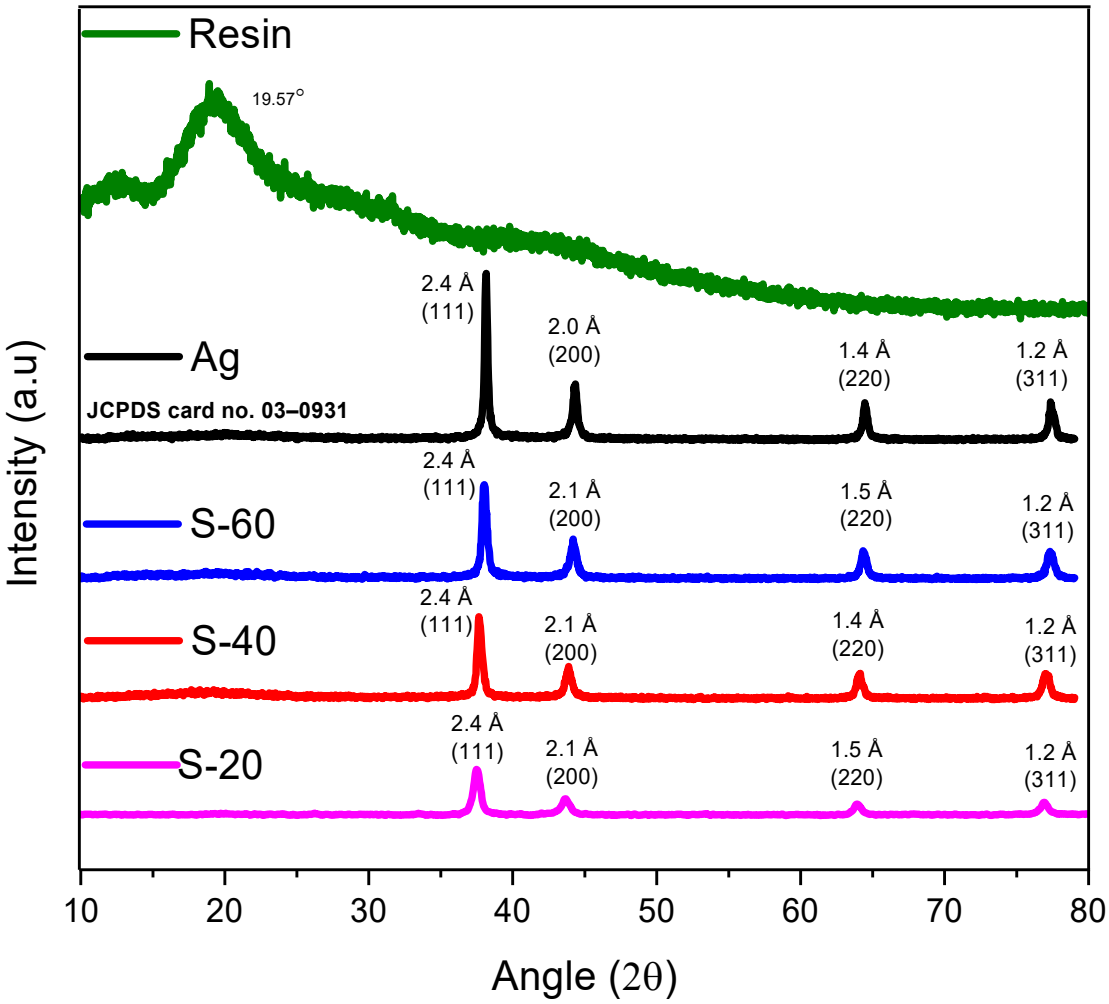

Figure 4. XRD pattern of Ag and Ag composites.

XRD spectra of ternary graphite-Ag-resin nanocomposites have revealed the successful synthesis of composites (Figure 5). For SG-20 composite 2θ and d-spacings values were found as 26.4° $d_{(002)}$ = 3.4 Å, 38.0° $d_{(111)}$ = 2.4 Å, 44.2° $d_{(200)}$ = 2.0 Å, 54.5° $d_{(004)}$ = 1.7 Å, 64.3° $d_{(220)}$ = 1.4 Å, 77.3° $d_{(311)}$ = 1.2 Å while SG-40 composite also have almost similar results 26.4° $d_{(002)}$ = 3.4 Å, 38.0° $d_{(111)}$ = 2.4 Å, 44.2° $d_{(200)}$ = 2.0 Å, 54.5° $d_{(004)}$ = 1.7 Å, 64.2° $d_{(220)}$ = 1.5 Å, 77.3° $d_{(311)}$ = 1.2 Å. Composite SG-60 has shown the diffraction signals as 26.4° $d_{(002)}$ = 3.4 Å, 38.0° $d_{(111)}$ = 2.4 Å, 44.2° $d_{(200)}$ = 2.0 Å, 54.4° $d_{(004)}$ = 1.7 Å, 64.3° $d_{(220)}$ = 1.4 Å, 77.3° $d_{(311)}$ = 1.2 Å. These results have shown no shifting of peaks thus have confirmed no oxide formation in any of the composite even by the curing of resin containing nanoparticles in situ.

Preprints (www.preprints.org) | NOT PEER-REVIEWED | Posted: 6 June 2023 doi:10.20944/preprints202306.0372.v1

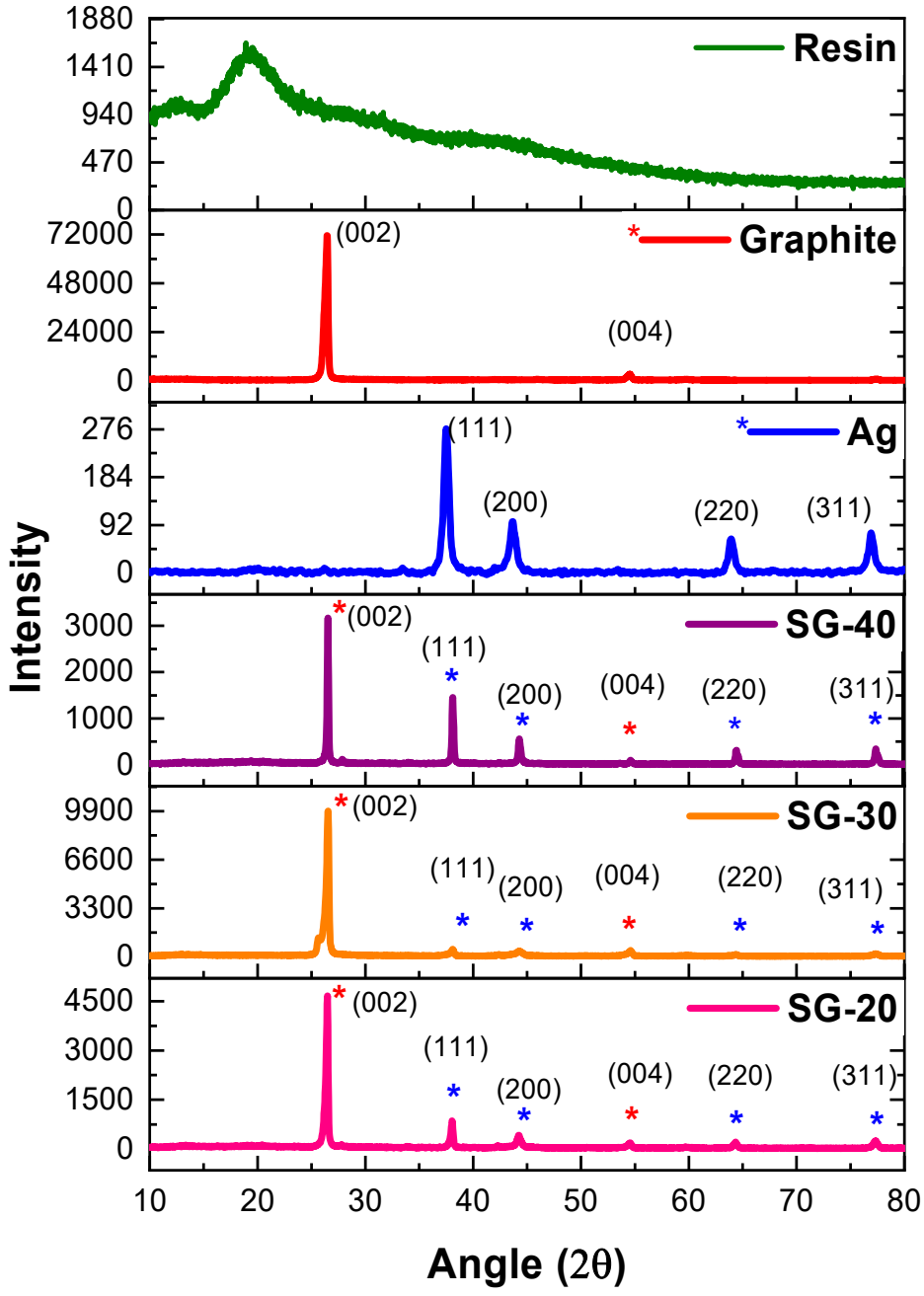

Figure 5. XRD results of resin, graphite, Ag, graphite-Ag-resin composites.

4.3. Scanning Electron Microscopy (SEM)

SEM micrographs have revealed micro-structured branching of resin, suggesting the 3D polymerization between phenol and furfural as shown in Figure 6 (a). Such high degree polymerization has also assured that there is no unreacted furfural or phenol left in the resin, suggesting no need of any type of curing agents, resulting in the impartment of thermosetting behavior along with crosslinking properties. Similar results were reported by Zeeshan et al. [24].

Preprints (www.preprints.org) | NOT PEER-REVIEWED | Posted: 6 June 2023 doi:10.20944/preprints202306.0372.v1

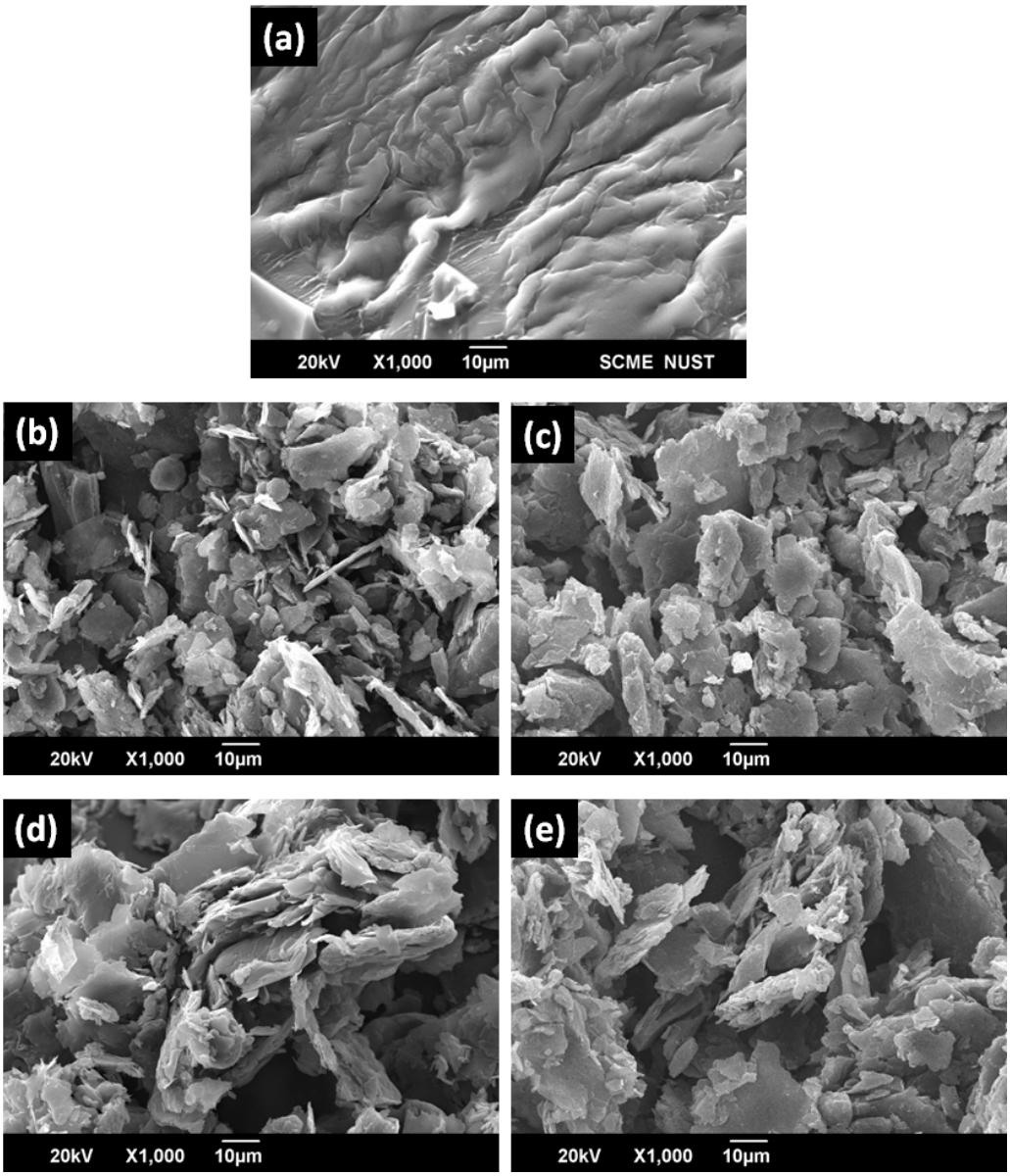

Figure 6. SEM micrograph of: (**a**) pure resin (**b**) Graphite, (**c**) G-20, (**d**) G-40, (**e**) G-60.

Figure 6 (b) shows graphite flakes SEM micrograph which are smooth, homogenous and in thin plate shape [28]. XRD and EDS have also confirmed the purity of graphite. Figure 6 (c-e) depicted SEM results of graphite-resin composites. Micrographs have indicated graphite dispersion on resin surface. As the graphite loading level increases the lighter region also increases confirming the conductive nature of graphite powder that was enhanced due to gold sputtering [24] while the non-conductive resin appeared as the darker region. Due to adhesive nature of resin graphite powder is well merged in the composite.

Figure 7 (a) shows silver nanoparticles SEM micrographs. These nanoparticles were fused spherical in shape of average size about 82 nm size. Such findings well match with the surface analysis study in reported literature [25]. The silver nanocomposites surface analysis in Figures 7 (b-d) has also indicated that spherical fused nanoparticles were well merged in the resins. The SEM has also confirmed that saturation of silver nanoparticles has also increased as the loading level of silver NPs has increased.

Preprints (www.preprints.org) | NOT PEER-REVIEWED | Posted: 6 June 2023 doi:10.20944/preprints202306.0372.v1

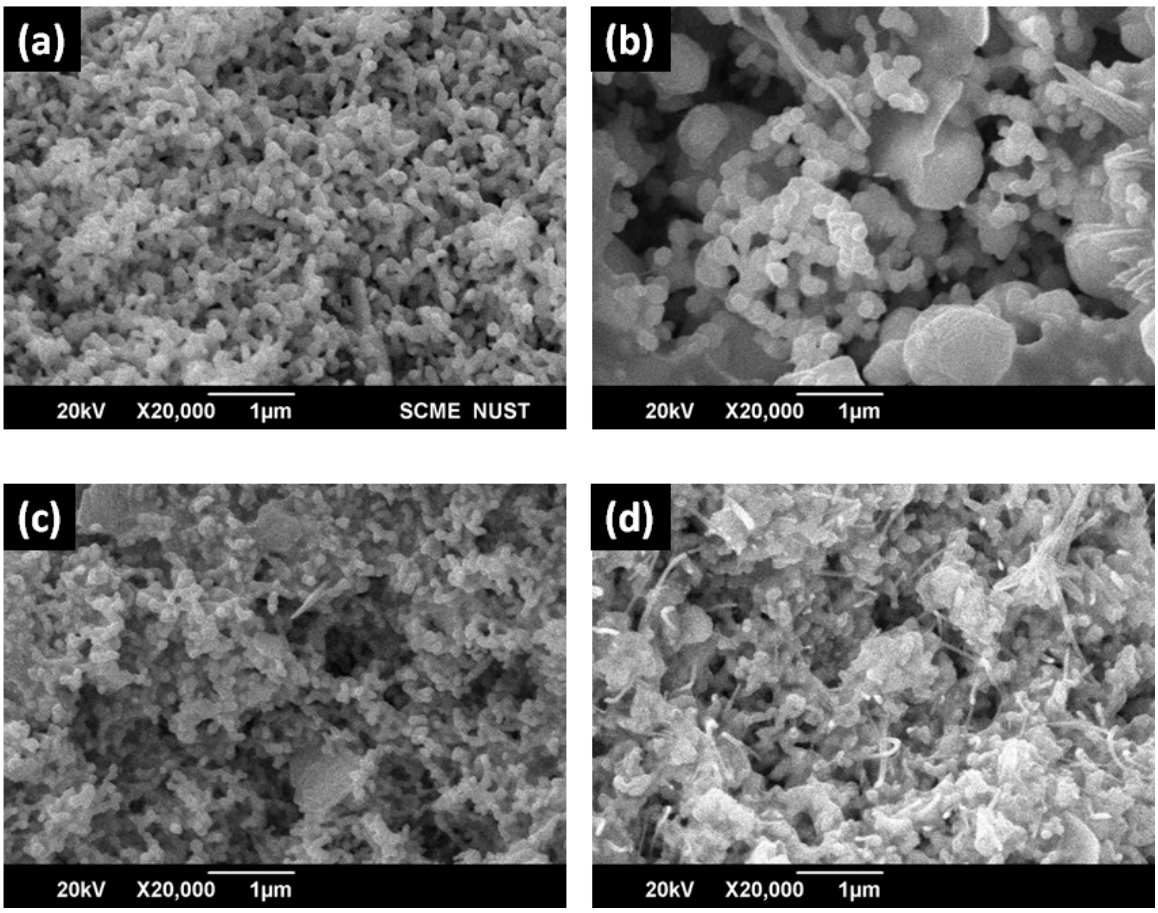

Figure 7. SEM analysis of Ag resin nanocomposite (**a**) Ag NPs, (**b**) S-20, (**c**) S-40, and (**d**) S-60.

The surface analysis of ternary composites constituted both nanoparticles blended with different weight percentages into resin have been studied and shown in Figure 8 along with the micrographs of all the pure precursors. Since these hybrid composites have both Ag NPs as well as graphite particles along with resin, therefore, larger aggregates become visible. Nano-structured silver particles were perfectly blended with the resin. All the silver-graphite composites exhibited complex 3D surface which is due to branching and polymerization of resin after curing.

Preprints (www.preprints.org) | NOT PEER-REVIEWED | Posted: 6 June 2023 doi:10.20944/preprints202306.0372.v1

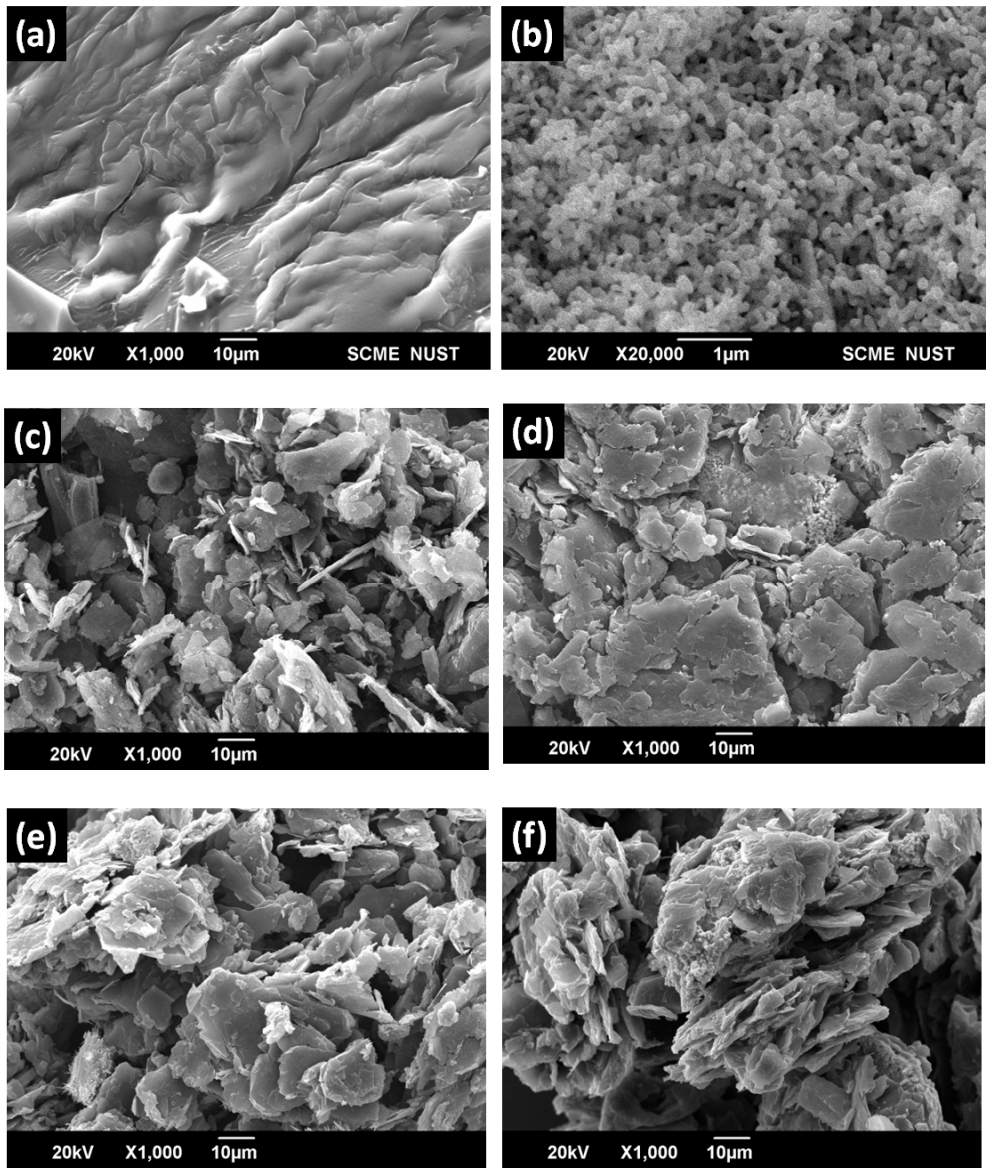

Figure 8. SEM results (a) resin, (b) silver nanoparticles, (c) graphite, (d) SG-20, (e) SG-30, and (f) SG-40.

The elemental mapping of pure resin is illustrated using Energy Dispersive X-Ray Spectroscopy shown in Figure 9 (a). Carbon appeared as the highest moiety while oxygen was detected as the second major elements. Both of these are backbone elements of resin. Sodium is also detected because NaOH was used in catalyst mixture. Pure Ag was detected as the single element in the elemental analysis as shown in Figure 9 (b). Elemental composition of graphite powder was also depicted in Figure 9 (c). The presence of 4.7 w/w % oxygen can be attributed to oxygen functionalities at surface. Figure 9 (d, e, f) shows the EDS results of all the graphite composites G-20, G-40, and G-60 respectively that only contained C, and O as the major element while sodium was used as the catalyst. The elemental composition of silver nanocomposites is also shown in Figure 9 . The successful preparation of all the composites was confirmed by the increase in the weight % of silver content which is represented in Figure 9 (g, h, i) as 25.4 w/w%, 45.4 w/w%, and 54.1 w/w % for S-20, S-40, and S-60 respectively. The graphite-silver composite is shown in Figure 9 (j, k, l) which verifies the successful blending of silver with graphite and resin. Elemental contents were found in agreement with the proportion of components (resin/graphite/Ag) employed in composite formation.

Preprints (www.preprints.org) | NOT PEER-REVIEWED | Posted: 6 June 2023 doi:10.20944/preprints202306.0372.v1

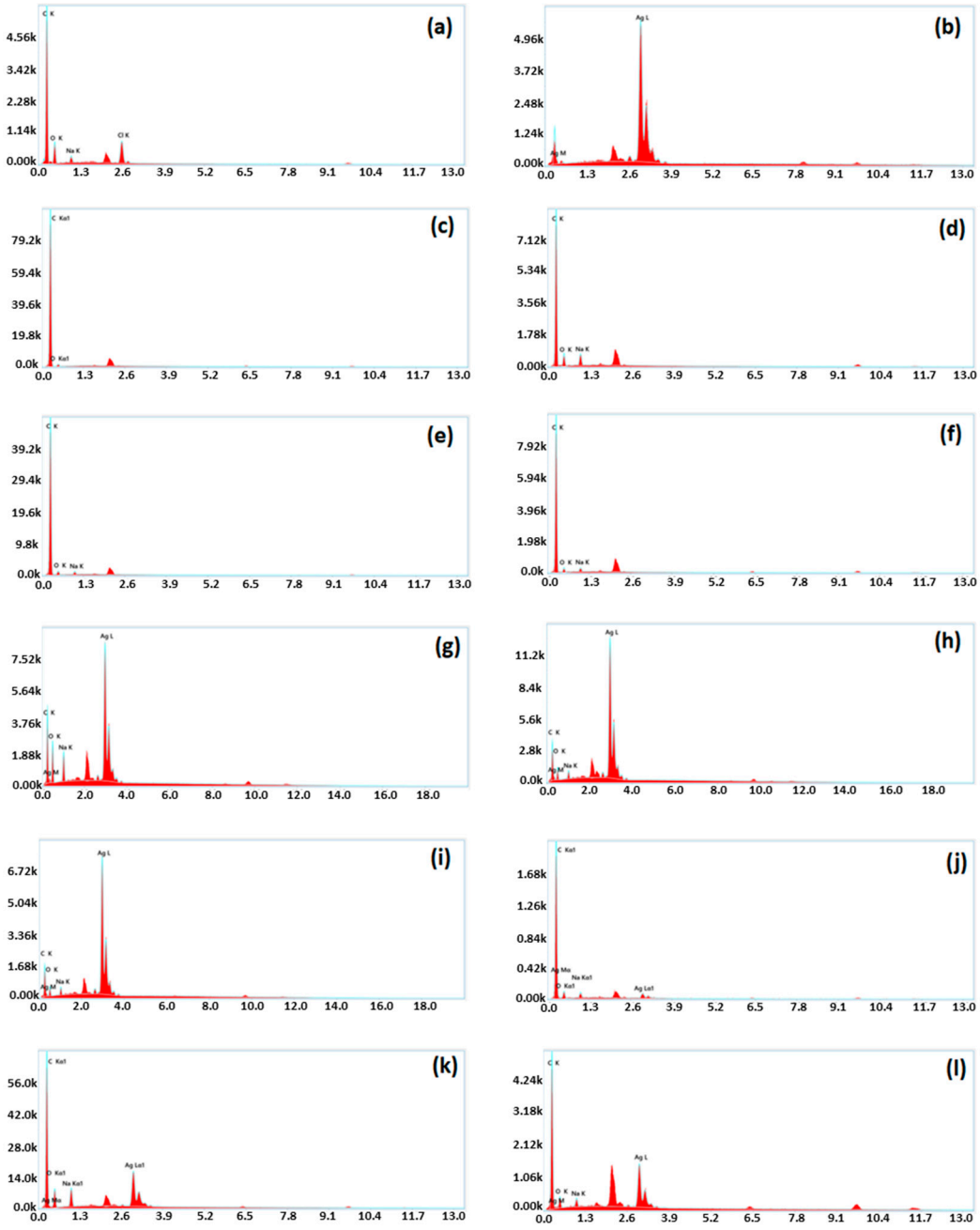

Figure 9. EDS results of (**a**) Pure resin (**b**) Ag NPs (**c**) Graphite (**d**) G-20 (**e**) G-40 (**f**) G-60 (**g**) S-20 (**h**) S-40 (**i**) S-60 (**j**) SG-20 (**k**) SG-30 (**l**) SG-40.

4.4. Thermogravimetric Analysis

Thermal stability behavior was checked for all pure resin, nanoparticles, and nanocomposites via TGA. For pure resin, onset temperature T_o (where decomposition started) was 96 °C while decomposition temperature T_f (where decomposition ended) was 727 °C. T_{deg} was 438 °C, the temperature at which maximum degradation was done. Likewise, the TGA values of pure graphite were 600 °C, 705 °C for T_o and T_f respectively. Its thermal stability range was 26 °C to 600 °C. Degradation temperature was increased from 438 °C to about 500 °C as the graphite powder was added. Detailed TGA results of binary composites of resin and graphite are described in Table 1 and Figure 10. The temperature up-to about 96 °C could also be related to the loss of water molecules, oligomers, and small residual monomers. While the temperature region from 96 °C to 727 °C results in overall degradation, in which chains break apart and different reaction regarding cross-linking

Preprints (www.preprints.org) | NOT PEER-REVIEWED | Posted: 6 June 2023 doi:10.20944/preprints202306.0372.v1

occurred. Therefore, those structures which were previously formed partially decompose, resulting in the formation of carbonaceous residue beyond the temperatures 727 °C. Similar trends were observed by Zeeshan et al [24].

Table 1. TGA results of graphite-resin composites.

Pure resin and nanocomposites	Temperature (^{0}C)		
	T_0	T_{deg}	T_f
Bagasse resin	96	438	727
Graphite	600	658	705
G-20	154	499	847
G-40	133	500	855
G-60	130	499	874

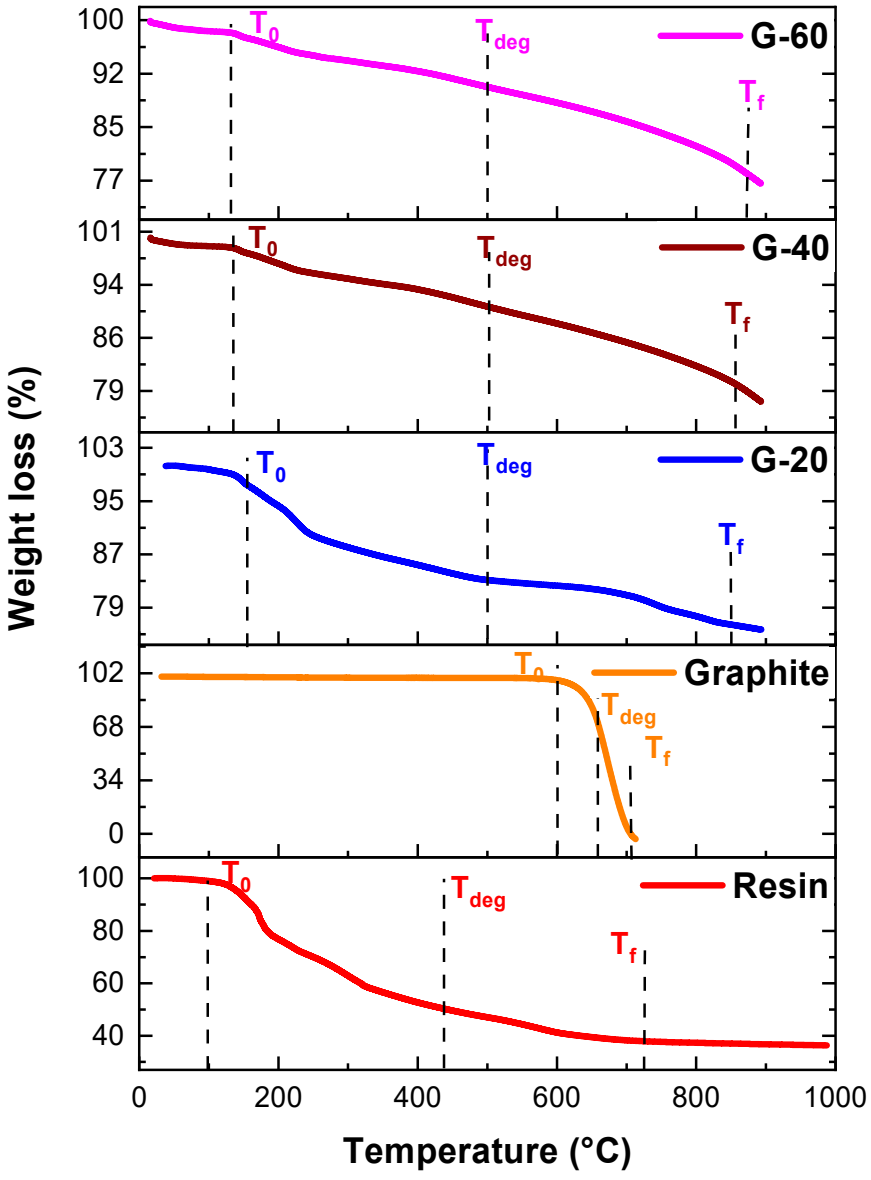

Figure 10. TGA analysis of resin, graphite, and graphite resin composite.

Figure 11 exhibits TGA curves for silver nanoparticles and their binary resin composites. Temperatures T_f, T_o and T_{deg} were 883 °C, 200 °C, and 549 °C respectively for silver nanoparticles. After blending with resin, their thermal stability was rechecked. It was observed that T_0 values have

Preprints (www.preprints.org) | NOT PEER-REVIEWED | Posted: 6 June 2023 doi:10.20944/preprints202306.0372.v1

increased from 96 °C to 117 °C, 127°C, and 122°C for S-20, S-40, and S-60 respectively because of silver nanoparticles which have increased thermal stability. Similarly, T_{deg} values were also increased from 438 °C to 499 °C, from resin to S-60 confirming thermal stability increases due to the incorporation of nanoparticles. (Table 2).

Table 2. TGA results of silver-resin nanocomposites.

Pure resin and nanocomposites	Temperature (⁰C)		
	T_0	T_{deg}	T_f
Bagasse resin	96	438	727
Ag	200	545	883
S-20	117	499	874
S-40	127	500	871
S-60	122	500	876

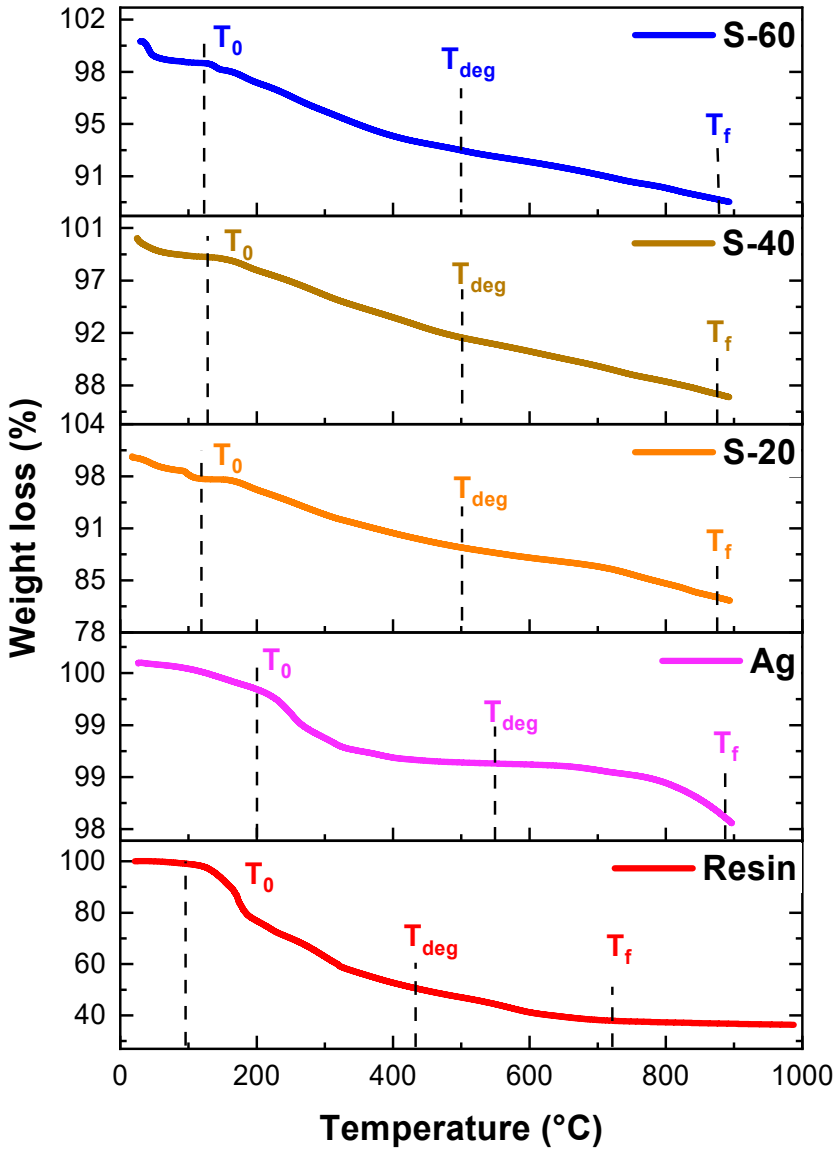

Figure 11. TGA graphs of resin, Ag, silver resin nanocomposite.

Figure 12 exhibits TGA curves for silver nanoparticles, graphite, and their ternary resin composites. It was observed that T_0 values of resin have increased from 96 °C to up to 120°C for all ternary resin composites. Whereas T_{deg} values were increased from 438 °C to 474 °C, 484 °C, and 512

Preprints (www.preprints.org) | NOT PEER-REVIEWED | Posted: 6 June 2023 doi:10.20944/preprints202306.0372.v1

°C for S-20, S-40, and S-60 respectively (Table 3, Figure 12). These results have shown that upon incorporation of silver and graphite nanoparticles there is a significant increase in thermal stability of ternary composites. These results also matches with conventional phenolic resins [29]. Thermogravimetric results exposed introduction of graphite and metallic nanoparticles into the resin has lowered the degradation rate that could be related for the increased in crosslinking between nanoparticles and resin.

Table 3. Graphite Ag resin nanocomposite.

Pure resin and nanocomposites	Temperature (°C)		
	T_0	T_{deg}	T_f
Bagasse resin	96	438	727
Graphite	600	658	705
Ag	200	545	883
SG-20	120	474	860
SG-30	120	484	866
SG-40	120	512	865

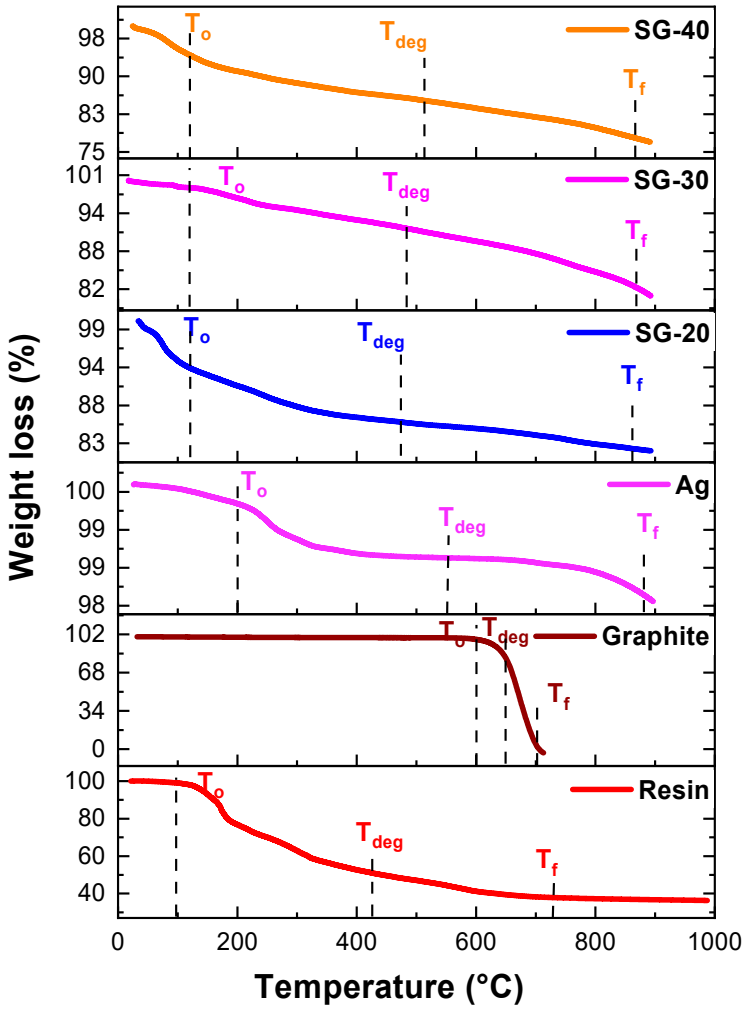

Figure 12. TGA graphs for Graphite/Ag/resin nanocomposites.

Preprints (www.preprints.org) | NOT PEER-REVIEWED | Posted: 6 June 2023 doi:10.20944/preprints202306.0372.v1

4.5. UV-DRS

A diffuse reflectance spectroscopic technique was used for the measurement of electrical conductivity. Band gap calculations were done using Tauc plot calculations. Pure graphite extracted from dry battery cells, has exhibited a bandgap energy value of about 3.5 eV. Similar value was reported by other researchers in the literature [30]. While resin exhibited a higher bandgap energy value of about 3.6 eV. All the graphite-resin composites have shown bandgap energy values slightly less than 3.5 eV. Thus, all graphite-resin composites are semi-conductors (Figure 13).

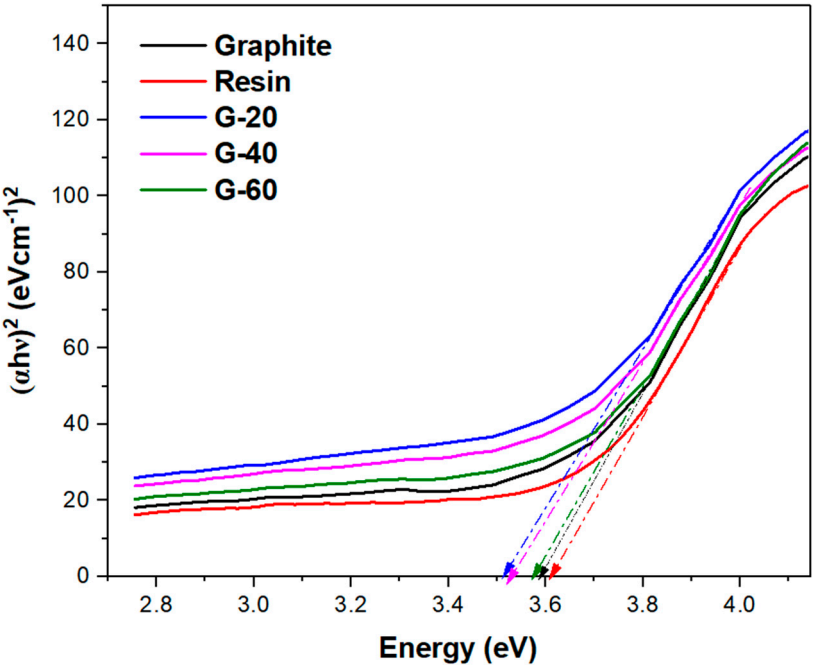

Figure 13. Tauc plot of graphite/resin composite.

Pure silver nanoparticles have exhibited a bandgap energy value of about 3.5 eV. Similar result was reported by AJ Das et al. [31]. All the silver-resin composites have shown bandgap energy values less than 3.5 eV. Thus, all silver-resin composites are semi-conductors (Figure 14).

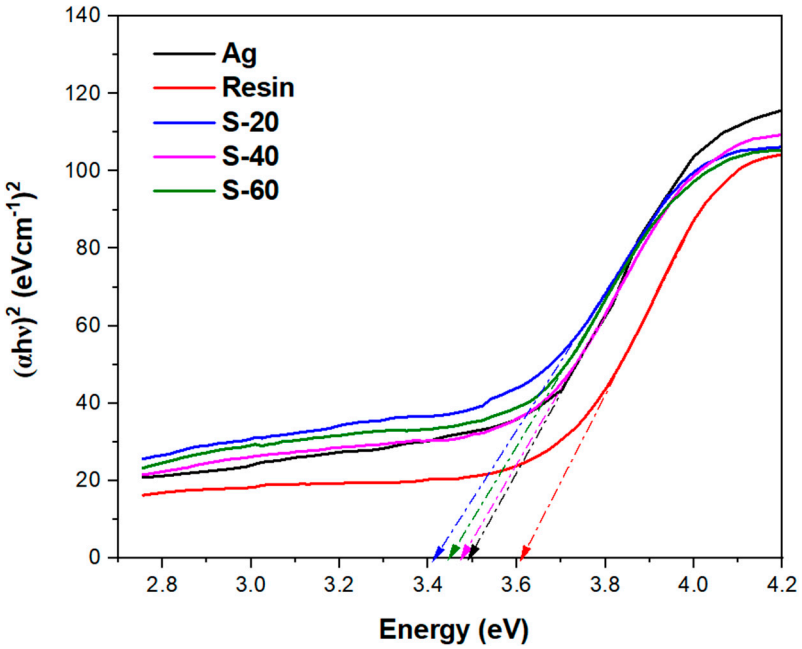

Figure 14. Tauc plot of Ag-resin composite.

Preprints (www.preprints.org) | NOT PEER-REVIEWED | Posted: 6 June 2023 doi:10.20944/preprints202306.0372.v1

The lowest bandgap energy value i.e., 3.1 eV was exhibited by SG-40 (Figure 15) Ag-graphite-resin nanocomposite. While the bandgap values for both nanocomposite SG-20 and SG-30 were about 3.3 eV which is slightly less compared to the silver bandgap energy value. The lowest bandgap energy value of SG-40 could be due to the reason that silver contains one valance electron in the electronic structure as well as the optimized 20 w/w% of graphite loading that has synergistically performed for electronic conduction. While 40 w/w% of resin aided perfectly in providing adhesiveness, fine, and uncracked cured texture.

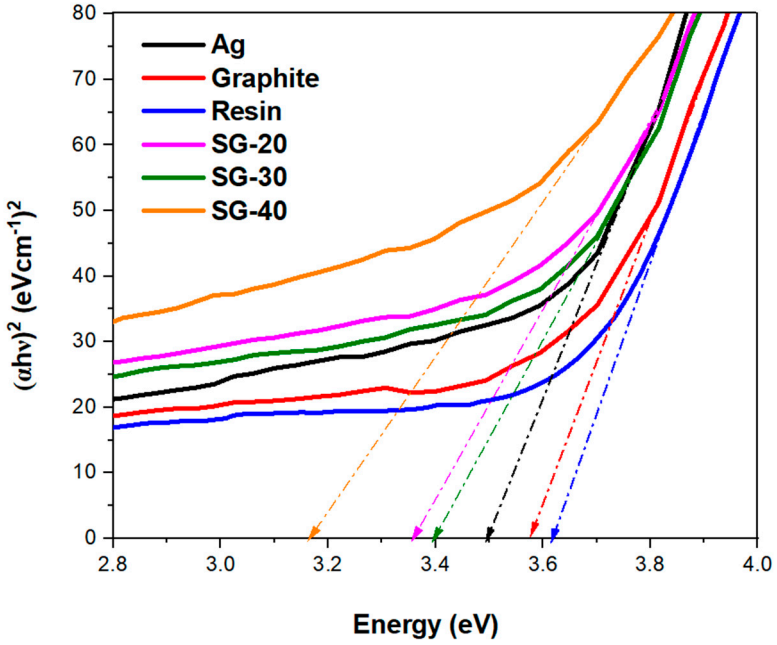

Figure 15. Tauc plot of Graphite-Ag-resin composite.

4.6. Four Probe Technique

The electrical conductivity of the composites was indirectly measured using a four-probe method. Figure 16 shows the electrical conductivity results of graphite-Ag-resin binary and ternary composites. Pure resin has exhibited poor conductivity of the order 2.6×10^{-4} Scm^{-1}, but conductivity was significantly increased up to 2.2×10^{-2} Scm^{-1} by 20 w/w% of graphite-resin composite. This value of electrical conductivity was further increased to about 5.6×10^{-2} Scm^{-1} and 3.92×10^{-1} Scm^{-1} with 40 w/w% and 60 w/w% of graphite resin composite respectively. Upon further addition of graphite, it hinders the mechanical stirring resulting in self-agglomeration and lumps formation due to voids, and spaces in graphite powder. In order to study electrical properties of resin, silver nanoparticles metallic filler was also loaded in different percentages. The conductivity of Ag-resin nanocomposite film was calculated as 1.72×10^{-1} Scm^{-1}, 2.75×10^{-1} Scm^{-1}, 3.92×10^{-1} Scm^{-1} upon addition of 20 w/w%, 40 w/w%, and 60 w/w% of Ag nanoparticles respectively, which is far greater than the conductivity results of Ag NPs in resin 2.48×10^{-2} Sm^{-1} reported by Ibrahim *et al*. [13]. These results have exhibited good electrical conductivities Ag-resin nanocomposite film compared to graphite-resin composite because Ag has lower ionization energy 7.57 eV while that of carbon is 11.26 eV. Therefore, Ag provides rapid flow of electrons just by applying less energy. Likewise, the highest conductivity was observed by SG-40 of about 8.26×10^{-1} Scm^{-1} as it consists of both silver and graphite nanoparticles in optimum concentration while 4.12×10^{-1} Scm^{-1}, 5.98×10^{-1} Scm^{-1} were calculated for SG-20 and SG-30 respectively. This optimized composite SG-40 comprised 40 w/w% Ag and 20 w/w% of graphite has furnished the best conductivity results. However, further enrichment causes nonhomogeneous mixing as well as difficulty in mechanical stirring. It is proposed that both silver and graphite nanoparticles act as junction in between polymeric chains of resin.

Preprints (www.preprints.org) | NOT PEER-REVIEWED | Posted: 6 June 2023 doi:10.20944/preprints202306.0372.v1

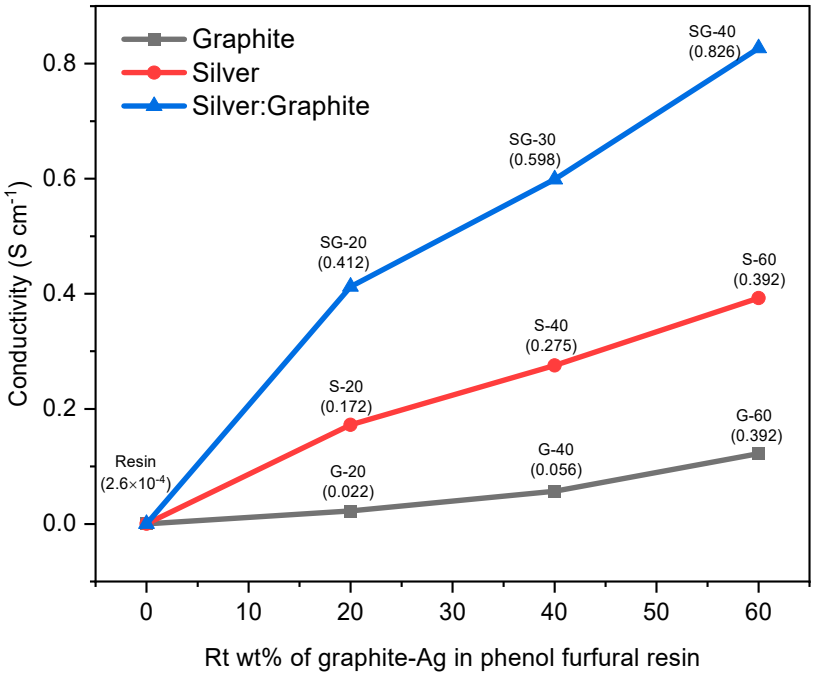

Figure 16. Electrical conductivity results of graphite-Ag-resin binary and ternary composites

5. Conclusion

Phenol furfural resin was successfully synthesized along with graphite and silver as nanofillers which have improved thermal and electrical features. Various hybrids of nanocomposites were well corroborated with the data analysis of SEM, XRD, FTIR, and EDS. Different ratios of conductive fillers (20 to 60 w/w %) were loaded in the polymerized matrix to obtain the optimized adhesion and electrical performance of films. Successful blending of graphite and silver particles up to 60 w/w% in resin was yielded, as beyond this mechanical stirring was difficult. Results showed a significant increase in the resin conductivity from 2.6 $\times 10^{-4}$ Scm^{-1} to 8.2 $\times 10^{-1}$ Scm^{-1} (SG-40) with band gap energy value of 3.1 eV, and thermal degradation T_{deg} from 438 ^{O}C to 512 °C. These results have shown that polymeric resin synthesized from bagasse and loaded with conductive nanoparticles, has good potential to be employed as electrically conductive adhesives.

6. Patents

This section is not mandatory but may be added if there are patents resulting from the work reported in this manuscript.

Author Contributions: Conceptualization, S.M.Z. and M.Z.A.; Methodology, M.Z.A. and S.M.Z; Formal analysis, S.M.Z and A.M; Writing—original draft preparation, S.M.Z; Writing—review and editing, A.M., M.B, and S.H.Z; Supervision, A.M.,f and A.K; All authors have read and agreed to the published version of the manuscript.

Funding: This research received no external funding.

Acknowledgments: Authors are thankful to o School of Chemical & Materials Engineering; U.S.-Pakistan Center for Advanced Studies in Energy of NUST; and Syed Babar Ali School of Science and Engineering Lahore University of Management Sciences. for extending their technical support to this research work.

Conflicts of Interest: The authors declare no conflict of interest.

References

1. Huber, G.W., S. Iborra, and A.J.C.r. Corma, *Synthesis of transportation fuels from biomass: chemistry, catalysts, and engineering*. 2006. **106**(9): p. 4044-4098.

2. Huber, G.W., J.N. Chheda, C.J. Barrett, and J.A.J.S. Dumesic, *Production of liquid alkanes by aqueous-phase processing of biomass-derived carbohydrates.* 2005. **308**(5727): p. 1446-1450.
3. Tondi, G. and T.J.P. Schnabel, *Bio-based polymers for engineered green materials*. 2020, MDPI. p. 775.
4. Zhang, Y., Y.-J. Heo, M. Park, and S.-J.J.P. Park, *Recent advances in organic thermoelectric materials: Principle mechanisms and emerging carbon-based green energy materials.* 2019. **11**(1): p. 167.
5. Hou, T., B. Wang, Z. Jia, H. Wu, D. Lan, Z. Huang, A. Feng, M. Ma, and G.J.J.o.M.S.M.i.E. Wu, *A review of metal oxide-related microwave absorbing materials from the dimension and morphology perspective.* 2019. **30**(12): p. 10961-10984.
6. Gao, Z., B. Xu, M. Ma, A. Feng, Y. Zhang, X. Liu, Z. Jia, and G.J.C.P.B.E. Wu, *Electrostatic self-assembly synthesis of ZnFe2O4 quantum dots (ZnFe2O4@ C) and electromagnetic microwave absorption.* 2019. **179**: p. 107417.
7. Kurlyandskaya, G., A. Safronov, T. Terzian, N. Volodina, I. Beketov, L. Lezama, and L.M.J.I.M.L. Prieto, *Fe 45 Ni 55 magnetic nanoparticles obtained by electric explosion of wire for the development of functional composites.* 2015. **6**: p. 1-4.
8. Scordo, G., V. Bertana, L. Scaltrito, S. Ferrero, M. Cocuzza, S.L. Marasso, S. Romano, R. Sesana, F. Catania, and C.F.J.M.T.C. Pirri, *A novel highly electrically conductive composite resin for stereolithography.* 2019. **19**: p. 12-17.
9. Ren, H.-M., Y. Guo, S.-Y. Huang, K. Zhang, M.M. Yuen, X.-Z. Fu, S. Yu, R. Sun, C.-P.J.A.a.m. Wong, and interfaces, *One-step preparation of silver hexagonal microsheets as electrically conductive adhesive fillers for printed electronics.* 2015. **7**(24): p. 13685-13692.
10. Guadagno, L., M. Raimondo, V. Vittoria, L. Vertuccio, C. Naddeo, S. Russo, B. De Vivo, P. Lamberti, G. Spinelli, and V.J.R.A. Tucci, *Development of epoxy mixtures for application in aeronautics and aerospace.* 2014. **4**(30): p. 15474-15488.
11. Novák, I. and I.J.E.P.J. Krupa, *Electro-conductive resins filled with graphite for casting applications.* 2004. **40**(7): p. 1417-1422.
12. Lopes, P.E., D. Moura, L. Hilliou, B. Krause, P. Pötschke, H. Figueiredo, R. Alves, E. Lepleux, L. Pacheco, and M.C.J.J.o.C.S. Paiva, *Mixed carbon nanomaterial/epoxy resin for electrically conductive adhesives.* 2020. **4**(3): p. 105.
13. Ibrahim, N. and M. Mustapha. *Electrical conductivity of silver conductive ink synthesized using chemical reduction method*. in *AIP Conference Proceedings*. 2020. AIP Publishing LLC.
14. Li, J.-X., Z.-X. Du, and R.-F.J.Z.f.K.-N.C.S. Bai, *Crystal structure of aqua-bis (5-bromo-6-methyl-picolinato-κ2N, O) zinc (II) dihydrate, C14H16Br2N2O7Zn.* 2020. **235**(1): p. 63-65.
15. Li, J.-X., Z.-X. Du, J. Wang, and X.J.Z.f.N.B. Feng, *Two mononuclear zinc (II) complexes constructed by two types of phenoxyacetic acid ligands: syntheses, crystal structures and fluorescence properties.* 2019. **74**(11-12): p. 839-845.
16. Feng, A., M. Ma, Z. Jia, M. Zhang, and G.J.R.a. Wu, *Fabrication of NiFe 2 O 4@ carbon fiber coated with phytic acid-doped polyaniline composite and its application as an electromagnetic wave absorber.* 2019. **9**(44): p. 25932-25941.
17. Li, J.-X. and Z.-X.J.J.o.C.S. Du, *A binuclear cadmium (II) cluster based on π··· π stacking and halogen··· halogen interactions: synthesis, crystal analysis and fluorescent properties.* 2020. **31**(2): p. 507-511.
18. Li, J.-X., Z.-X. Du, and X.J.Z.f.N.B. Feng, *A new binuclear NiII complex with tetrafluorophthalate and 2, 2′-bipyridine ligands: synthesis, crystal structure and magnetic properties.* 2019. **74**(11-12): p. 833-838.
19. Suherman, H., Y. Mahyoedin, E. Septe, and R.J.A.M.S. Rizade, *Properties of graphite/epoxy composites: the in-plane conductivity, tensile strength and Shore hardness.* 2019. **6**(2): p. 165-173.
20. Dhakate, S., R. Mathur, B. Kakati, and T.J.I.J.o.H.E. Dhami, *Properties of graphite-composite bipolar plate prepared by compression molding technique for PEM fuel cell.* 2007. **32**(17): p. 4537-4543.
21. Yu, A., M.E. Itkis, E. Bekyarova, and R.C.J.A.P.L. Haddon, *Effect of single-walled carbon nanotube purity on the thermal conductivity of carbon nanotube-based composites.* 2006. **89**(13): p. 133102.
22. Tang, Z., Y. Liu, Y. Zhang, Z. Sun, W. Huang, Z. Chen, X. Jiang, and L.J.N. Zhao, *Design and Synthesis of Functional Silane-Based Silicone Resin and Application in Low-Temperature Curing Silver Conductive Inks.* 2023. **13**(6): p. 1137.
23. Dar, R.A., N.G. Khare, D.P. Cole, S.P. Karna, and A.K.J.R.A. Srivastava, *Green synthesis of a silver nanoparticle–graphene oxide composite and its application for As (III) detection.* 2014. **4**(28): p. 14432-14440.

24. Asad, M.Z., A. Mahmood, and S.T.J.P. Hussain Shah, *Phenol-Furfural Resin/Montmorillonite Based High-Pressure Green Composite from Renewable Feedstock (Saccharum munja) with Improved Thermo-Mechanical Properties.* 2020. **12**(7): p. 1562.
25. Tantawy, H.R., A.A. Nada, A. Baraka, and M.A.J.A.S.S.A. Elsayed, *Novel synthesis of bimetallic Ag-Cu nanocatalysts for rapid oxidative and reductive degradation of anionic and cationic dyes.* 2021. **3**: p. 100056.
26. Guo, L., B. Zhang, S. Bai, X. Ma, and Z.J.e.-P. Wang, *Synthesis and application of functionalized ionic liquids as solvent to corn stalk for phenolic resin modification.* 2015. **15**(3): p. 195-201.
27. Agasti, N. and N.J.A.J.o.N. Kaushik, *One pot synthesis of crystalline silver nanoparticles.* 2014. **2**(1): p. 4-7.
28. Rew, Y., A. Baranikumar, A.V. Tamashausky, S. El-Tawil, P.J.C. Park, and B. Materials, *Electrical and mechanical properties of asphaltic composites containing carbon based fillers.* 2017. **135**: p. 394-404.
29. Puglia, D., J. Kenny, L. Manfredi, and A.J.M.E.-M.-. Vázquez, *Influence of the chemical composition on the thermal degradation and fire resistance of resol type phenolic resins.* 2001. **12**(1): p. 55-72.
30. George, P. and P.J.A. Chowdhury, *Complex dielectric transformation of UV-vis diffuse reflectance spectra for estimating optical band-gap energies and materials classification.* 2019. **144**(9): p. 3005-3012.
31. Das, A., R. Kumar, S. Goutam, and S.J.J.B.B.S. Sagar, *Sunlight irradiation induced synthesis of silver nanoparticles using glycolipid bio-surfactant and exploring the antibacterial activity.* 2016. **6**(5).